Pramana – J. Phys. (2019) 93:96
https://doi.org/10.1007/s12043-019-1838-8

Entropy generation minimisation: Nonlinear mixed convective flow of Sisko nanofluid

TASAWAR HAYAT[1,2], FARIA MASOOD[1], SUMAIRA QAYYUM[1,*] and AHMED ALSAEDI[2]

[1]Department of Mathematics, Quaid-I-Azam University 45320, Islamabad 44000, Pakistan
[2]Nonlinear Analysis and Applied Mathematics (NAAM) Research Group, Department of Mathematics, Faculty of Science, King Abdulaziz University, Jeddah 21589, Saudi Arabia
[*]Corresponding author. E-mail: sumaira@math.qau.edu.pk

MS received 21 February 2019; revised 23 May 2019; accepted 31 May 2019

Abstract. Two-dimensional magneto-Sisko nanofluid flow bounded by nonlinearly stretching sheet is studied. Thermophoretic diffusion and Brownian motion effects are also scrutinised. Additionally, impacts of activation energy, chemical reaction and nonlinear convection are considered. The purpose of this study is to analyse entropy generation in the Sisko fluid model. Suitable transformations are used to reduce the governing equation of motion, concentration and temperature. Effects of some pertinent variables on skin friction coefficient, temperature, velocity, concentration and Nusselt number are graphically presented. Clearly, for larger Brownian and thermophoresis parameters, the temperature increases while concentration distribution decreases with Brownian parameter. Bejan number is maximum away from the sheet in the case of shear thickening fluids while it approaches zero for shear thinning fluids.

Keywords. Sisko nanofluid; magnetohydrodynamics; nonlinear mixed convection; entropy generation; activation energy; chemical reaction.

PACS Nos 47.10.A; 47.15.G; 47.27.Ak; 47.10.FW

1. Introduction

Discussion on non-Newtonian flow is a hot topic for researchers nowadays. Such types of flow can be seen in ketchup and toothpaste, certain oils, polymers, etc. Non-Newtonian materials are also used in many industrial and engineering processes. They have various characteristics and attributes and no single relation is enough to describe such materials. Here, we considered the Sisko [1] fluid model which has characteristics of shear thinning and shear thickening. It comprises both viscous and power-law models. A few work on Sisko fluid can be seen in [2–11].

Nanoparticles have a key role in any substance and its molecular/atomic structure. Nanoparticles are very good cooling agents due to their higher thermal conductance and lower molecular weight. Nanofluids are commonly used in different biomedical and technical devices such as fuel cells, radiators, nanomedication and nuclear reactors. Choi [12] gave the concept of nanomaterial in continuous phase liquid and he experimentally proved that such materials enhanced the thermal characteristics of continuous phase liquids. Series solution for stagnation-point nanofluid flow on stretching surface was discussed by Mustafa *et al* [13]. Zheng *et al* [14] examined the temperature jump and wall slip effects over a deforming surface for radiative heat transfer in nanofluid flows. For series solution, they employed a homotopy technique. Kellor–Box method was employed by Mustafa *et al* [15] just to discuss three different types of nanofluids for classical Bödewadt flow. Lin *et al* [16] utilised five different types of nanoparticles to discuss pseudoplastic nanofluids of variable thermal conductivity for Marangoni convection flow. Mahanthesh *et al* [17] considered the magnetohydrodynamics (MHD) nanofluid flow by a bidirectional nonlinear stretching sheet. Yin *et al* [18] studied the heat transport of nanomaterials over a rotating disk. Kumar *et al* [19] discussed the temperature-dependent thermal conductivity on fractional model for convective radial fins. Pandey and Kumar [20] examined the heat rate towards a stretching cylinder in copper–water nanomaterial flow. For computational results they use the RKF45 technique. Volume fraction is taken as 0–6%.

Published online: 04 October 2019

Furthermore, for increasing values of volume fraction parameter, the temperature profile enhances. He noticed a good agreement by comparing the present outcomes with the previously available articles. Kumar *et al* [21,22] studied the nanofluid flow in the presence of double diffusion, chemical reaction and thermal radiation.

In mixtures, when there are species with different concentrations, then mass transfer occurs. These species transport themselves from higher to lower concentration region in the mixture. Activation energy is actually the least obligatory energy, which a reactant must have before the chemical reaction takes place. In a porous space, natural convection binary mixture flow with activation energy is examined by Bestman [23]. Under the influence of activation energy and *n*th-order reaction, the unsteady natural convection flow was studied by Makinde *et al* [24]. In the presence of activation energy, Malique [25] studied the endothermic/exothermic reaction in mixed convection flows. Abbas *et al* [26] investigated the Casson fluid flow with activation energy and binary chemical reaction. Shafique *et al* [27] discussed the rotating viscoelastic flow subject to chemical reaction with activation energy. Unsteady rotating binary fluid flow was examined by Awad *et al* [28] over an impulsively stretched surface utilising the modified Arrhenius function.

In a thermodynamical system, chemical reactions between the solid surface and fluid viscosity and frictional forces are the major factors of entropy generation and energy loss. Entropy generation determines the irreversibility of viscous dissipation, and heat and mass transfer irreversibility. To increase the efficiency of any heat transfer process, entropy generation minimisation (EGM) is used as an effective tool. In different thermal engineering systems, such as chillers, air separators, chemicals, reactors and electrochemicals, EGM is applied. Irreversibility occurs inside the cavity during the convection process. EGM is used to conserve the energy and to reduce or overcome the process of irreversibility. First of all, Bejan [29] attempted the EGM and he used thermodynamics second law. Hayat *et al* [30] analysed the effect of entropy generation in MHD radiative flow by a rotating disk. The shape effects of copper nanoparticles were discussed by Ellahi *et al* [31] on entropy generation. Three-dimensional MHD viscous fluid flow was considered by Butt and Ali [32] to study the heat transfer and entropy generation over a stretching surface. To study viscous dissipation and entropy generation, Guo *et al* [33] considered the curved microchannel. Some relevant attempts in this direction can be seen in refs [34–38].

The main aim of the present study is to examine the effects of activation energy on nonlinear mixed convected flow of magnetic Sisko nanofluid over a stretching sheet. Homotopy technique [39–50] is used to solve this system. Convergent solutions are obtained. The effects of interesting parameters on velocity, temperature, concentration, entropy generation, Bejan number, Nusselt number and skin friction coefficient are discussed using graphs.

2. Modelling

Two-dimensional Sisko nanofluid flow in the presence of nonlinear mixed convection is discussed. Stretching sheet with velocity $u = cx^s$ causes disturbance in fluid, where $s \succ 0$ signifies the stretching rate of the surface and c is a non-negative real number (see figure 1). During the flow, we examine the entropy generation.

Conservation equations are [1,2,4,5,8,9]:

$$\frac{\partial \check{u}}{\partial x} + \frac{\partial \check{v}}{\partial y} = 0, \tag{1}$$

$$\check{u}\frac{\partial \check{u}}{\partial x} + \check{v}\frac{\partial \check{u}}{\partial y} = \frac{a}{\rho}\frac{\partial^2 \check{u}}{\partial y^2} - \frac{b}{\rho}\frac{\partial}{\partial y}\left(-\frac{\partial \check{u}}{\partial y}\right)^n - \frac{\sigma}{\rho}\check{B}_0^2\check{u} + g(\Lambda_1(\check{T} - \check{T}_\infty) + \Lambda_2(\check{T} - \check{T}_\infty)^2) + g(\Lambda_3(\check{C} - \check{C}_\infty) + \Lambda_4(\check{C} - \check{C}_\infty)^2), \tag{2}$$

$$\check{u}\frac{\partial \check{T}}{\partial x} + \check{v}\frac{\partial \check{T}}{\partial y} = \alpha\frac{\partial^2 \check{T}}{\partial y^2} + \tau\left[D_B\frac{\partial \check{T}}{\partial y}\frac{\partial \check{C}}{\partial y} + \frac{D_{\check{T}}}{\check{T}_\infty}\left(\frac{\partial \check{T}}{\partial y}\right)^2\right], \tag{3}$$

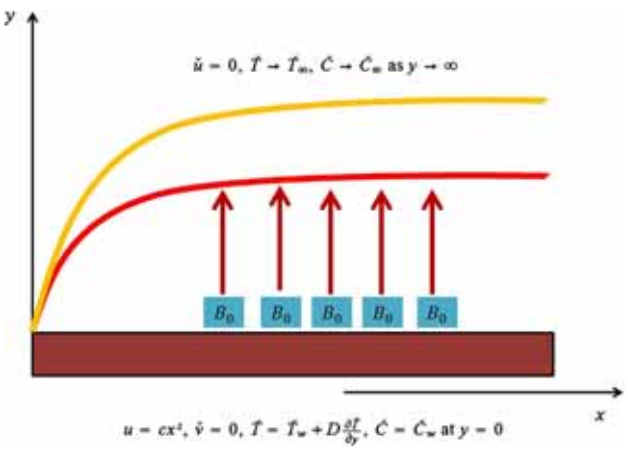

Figure 1. Flow geometry.

$$\breve{u}\frac{\partial \breve{C}}{\partial x}+\breve{v}\frac{\partial \breve{C}}{\partial y}=D_{\mathrm{B}}\frac{\partial^2 \breve{C}}{\partial y^2}+\frac{D_{\breve{T}}}{T_\infty}\frac{\partial^2 \breve{T}}{\partial y^2}$$
$$-k_{\mathrm{r}}^2(\breve{C}-\breve{C}_\infty)\left(\frac{\breve{T}}{\breve{T}_\infty}\right)^{n^*}\exp\left(\frac{-E_{\mathrm{a}}}{\kappa \breve{T}}\right), \tag{4}$$

where u, v are the velocities in the x, y direction, respectively. $\breve{T}$ is the temperature of the fluid, a denotes the viscosity at high shear rate while b denotes a consistency index, both are material constants. n is a power-law index, σ is the electrical conductivity, ρ is the density, D_{B} and D_{T} are the Brownian and thermophoretic diffusions, τ is the ratio between heat capacity of the base fluid and nanoparticle material, k_{r}^2 is the reaction rate, E_{a} is the activation energy and $\kappa = 8.61\times10^{-5}$ eV/K is the Boltzmann constant and n^* is the fitted rate constant.

For the present flow, the boundary conditions are

$$\tilde{u}=cx^s,\quad \breve{v}=0,\quad \breve{T}=\breve{T}_w+D\frac{\partial \breve{T}}{\partial y},$$
$$\breve{C}=\breve{C}_w \quad \text{at} \quad y=0,$$
$$\breve{u}=0,\quad \breve{T}\to\breve{T}_\infty,\quad \breve{C}\to\breve{C}_\infty \quad \text{as} \quad y\to\infty. \tag{5}$$

Suitable transformations chosen for this type of flow are

$$u=cx^s\breve{f}'(\eta),$$
$$v=-\frac{U_w}{n+1}\mathrm{Re}_b^{-1/(n+1)}[(s(2n-1)+1)\breve{f}(\eta)$$
$$+(s(2-n)-1)\eta\breve{f}'(\eta)],$$
$$\eta=\frac{y}{x}\mathrm{Re}_b^{1/(n+1)},\quad \breve{\theta}(\eta)=\frac{\breve{T}-\breve{T}_\infty}{\breve{T}_w-\breve{T}_\infty},$$
$$\breve{\phi}(\eta)=\frac{\breve{C}-\breve{C}_\infty}{\breve{C}_w-\breve{C}_\infty}. \tag{6}$$

Equations (2)–(5) take the form

$$A\breve{f}'''-n(-\breve{f}'')^{n-1}\breve{f}'''-s\breve{f}'^2$$
$$+\frac{(s(2n-1)+1)}{n+1}\breve{f}\breve{f}''-M\breve{f}'$$
$$+\lambda(1+\beta_t\breve{\theta})\breve{\theta}+\lambda N^*(1+\beta_c\breve{\phi})\breve{\phi}=0, \tag{7}$$

$$\breve{\theta}''+\mathrm{Pr}\frac{(s(2n-1)+1)}{n+1}\breve{f}\breve{\theta}'+Nb\breve{\theta}'\breve{\phi}'+Nt\breve{\theta}'^2=0, \tag{8}$$

$$\breve{\phi}''+\mathrm{Pr\,Le}\frac{(s(2n-1)+1)}{n+1}\breve{f}\breve{\phi}'+\frac{Nt}{Nb}\breve{\theta}''$$
$$-\sigma\,\mathrm{Le\,Pr}(1+\delta\breve{\theta})^{n^*}\exp\left(\frac{-E}{1+\delta\breve{\theta}}\right)\breve{\phi}=0, \tag{9}$$

with boundary conditions

$$\breve{f}'(0)=1,\quad \breve{\phi}(0)=1,\quad \breve{f}(0)=0,$$
$$\breve{\theta}(0)=1+\gamma\breve{\theta}'(0),$$
$$\breve{f}'(\infty)\to0,\quad \breve{\phi}(\infty)\to0,\quad \breve{\theta}(\infty)\to0, \tag{10}$$

where

$$Nt=\frac{\tau D_{\mathrm{T}}(\breve{T}_w-\breve{T}_\infty)}{\alpha\breve{T}_\infty},\quad \delta=\frac{\breve{T}_w-\breve{T}_\infty}{\breve{T}_\infty},$$
$$\gamma=\frac{D\mathrm{Re}_b^{1/(n+1)}}{x},\quad \mathrm{Gr}=\frac{\rho^2 g\Lambda_1(\breve{T}_w-\breve{T}_\infty)x^3}{a^2},$$
$$\mathrm{Gr}^*=\frac{\rho^2 g\Lambda_3(\breve{C}_w-\breve{C}_\infty)x^3}{a^2},\quad M=\frac{\sigma B_0^2 x}{\rho U_w},$$
$$\beta_{\mathrm{t}}=\frac{\Lambda_2}{\Lambda_1}(\breve{T}_w-\breve{T}_\infty),\quad \beta_{\mathrm{c}}=\frac{\Lambda_4}{\Lambda_3}(\breve{C}_w-\breve{C}_\infty),$$
$$Nb=\frac{\tau D_{\mathrm{B}}}{\alpha}(\breve{C}_w-\breve{C}_\infty),\quad N^*=\frac{\mathrm{Gr}^*}{\mathrm{Gr}},$$
$$\lambda=\frac{\mathrm{Gr}}{(\mathrm{Re}_a)^2},\quad \mathrm{Re}_a=\frac{\rho x U_w}{a},\quad \mathrm{Re}_b=\frac{\rho x^n U_w^{2-n}}{b},$$
$$\sigma=\frac{k_{\mathrm{r}}^2}{cx^{s-1}},\quad \mathrm{Le}=\frac{\alpha}{D_{\mathrm{B}}},\quad \mathrm{Pr}=\frac{cx^{s+1}}{\alpha}\mathrm{Re}_b^{-2/(n+1)}. \tag{11}$$

Here Nt indicates the thermophoresis parameter, σ is the dimensionless reaction rate, δ is the temperature difference parameter, E is the dimensionless activation energy, Nb is the Brownian diffusion parameter, Pr is the Prandtl number, Re_a and Re_b are the local Reynold numbers, Gr and Gr* are the Grashof numbers in terms of temperature and concentration, β_{t} and β_{c} are the nonlinear convection variables in terms of temperature and concentration, λ is for the mixed convection parameter, M is the the Hartmann number, N^* is the ratio of concentration to thermal buoyancy forces, γ is the thermal slip parameter and Le is the Lewis number.

Now the temperature and velocity gradients are defined as

$$\mathrm{Nu}_x=\frac{xq_w}{k(\breve{T}_w-\breve{T}_\infty)},\quad C_{\hat{f}_x}=\frac{2\tau_w}{\rho(U_w)^2}, \tag{12}$$

in which q_w and τ_w are

$$q_w=\left[-k\left(\frac{\partial \breve{T}}{\partial y}\right)\right]_{y=0}, \tag{13}$$

$$\tau_w=\left[\left(a\left(\frac{\partial \breve{u}}{\partial y}\right)+b\left(\frac{\partial \breve{u}}{\partial y}\right)^n\right)\right]_{y=0}. \tag{14}$$

Nusselt number and skin friction coefficient in dimensionless form are

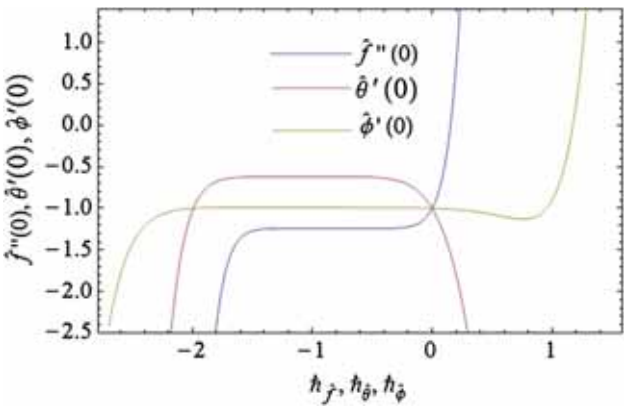

Figure 2. $\hbar$-curves of $\tilde{f}''(0)$, $\tilde{\theta}'(0)$ and $\tilde{\phi}'(0)$.

$$(\mathrm{Re})_b^{-1/(n+1)}\mathrm{Nu}_x = -\check{\theta}'(0), \tag{15}$$

$$\frac{1}{2}(\mathrm{Re})^{1/(n+1)}C_{f_x} = [A\check{f}''(0) - (-\check{f}''(0))^n]. \tag{16}$$

3. Solutions

Auxiliary linear operators and initial approximations are:

$$\mathcal{L}_{\check{f}}(\check{f}) = \check{f}''' - \check{f}', \quad \mathcal{L}_{\check{\theta}}(\check{\theta}) = \check{\theta}'' - \check{\theta},$$
$$\mathcal{L}_{\check{\phi}}(\check{\phi}) = \check{\phi}'' - \check{\phi}, \tag{17}$$
$$\check{f}_0(\xi) = 1 - \exp(-\xi), \quad \check{\phi}_0(\xi) = \exp(-\xi),$$
$$\check{\theta}_0(\xi) = \frac{1}{1+\gamma}\exp(-\xi) \tag{18}$$

with

$$\mathcal{L}_{\check{f}}(\check{f})[d_1 + d_2\mathrm{e}^{\xi} + d_3\mathrm{e}^{-\xi}] = 0,$$
$$\mathcal{L}_{\check{\phi}}(\check{\phi})[d_6\mathrm{e}^{\xi} + d_7\mathrm{e}^{-\xi}] = 0,$$
$$\mathcal{L}_{\check{\theta}}(\check{\theta})[d_4\mathrm{e}^{\xi} + d_5\mathrm{e}^{-\xi}] = 0, \tag{19}$$

where d_i (i =1–7) are constants.

4. Convergence analysis

Convergence region is adjusted with the help of auxiliary parameters $\hbar_{\check{f}}$, $\hbar_{\check{\theta}}$ and $\hbar_{\check{\phi}}$ by using the homotopy analysis method (HAM). To obtain the convergent solution, the admissible values of these parameters are essential. At 20th order of deformation, figure 2 is portrayed for $\hbar$-curves. Convergent ranges of admissible values for these parameters are $-1.2 \le \hbar_{\check{f}} \le -0.1$, $-1.3 \le \hbar_{\check{\theta}} \le -0.1$ and $1.5 \le \hbar_{\check{\phi}} \le -0.5$. Table 1 demonstrates the convergence of $\check{f}''(0)$, $\check{\theta}'(0)$ and $\check{\phi}'(0)$. It is observed that in our present analysis, convergence starts from 28th order of approximations.

Table 1. Numerical values for $\tilde{f}''(0)$, $\tilde{\theta}'(0)$ and $\tilde{\phi}'(0)$.

Order of approximation	$-\hat{f}''(0)$	$-\hat{\theta}'(0)$	$-\hat{\phi}'(0)$
1	1.1746	0.78438	0.99849
8	1.2398	0.62055	0.99634
17	1.2398	0.62101	0.99488
24	1.2398	0.62101	0.99401
30	1.2398	0.62101	0.99401
40	1.2398	0.62101	0.99401
50	1.2398	0.62101	0.99401

5. Entropy generation

Entropy generation actually determines the irreversibility of viscous dissipation, and heat and mass transfer irreversibility. To increase the efficiency of any heat transfer process, EGM is used as an effective tool.

In dimensional form, the entropy generation equation is

$$S_G = \frac{k}{T_\infty^2}\left[\frac{\partial \check{T}}{\partial y}\right]^2 + \frac{1}{\check{T}_\infty}\left[a\left(\frac{\partial \check{u}}{\partial y}\right)^2 + b\left(-\frac{\partial \check{u}}{\partial y}\right)^{n+1}\right] + \frac{R^* D}{\check{T}_\infty}\left[\frac{\partial \check{T}}{\partial y}\frac{\partial \check{C}}{\partial y}\right] + \frac{R^* D}{\check{C}_\infty}\left[\frac{\partial \check{C}}{\partial y}\right]^2 + \frac{\sigma}{\check{T}_\infty}B_0^2\check{u}^2. \tag{20}$$

After transformations eq. (20) becomes

$$N_G = (\mathrm{Re}_b)^{2/(n+1)} \times \left[\delta\check{\theta}'^2 + (\mathrm{Br})\check{f}''^2 + L\alpha_1\check{\theta}'\check{\phi}' + \frac{L}{\delta}\alpha_1^2\check{\phi}'^2\right] + M(\mathrm{Re}_a)(\mathrm{Br})\check{f}'^2 + (\mathrm{Re}_a)(\mathrm{Br})(-\check{f}'')^{n+1}. \tag{21}$$

The dimensionless parameters are

$$\alpha_1 = \frac{\check{C}_w - \check{C}_\infty}{\check{C}_\infty}, \quad \delta = \frac{\check{T}_w - \check{T}_\infty}{\check{T}_\infty}, \quad \mathrm{Br} = \frac{aU_w^2}{k\Delta\check{T}},$$
$$N_G = \frac{\check{T}_\infty S_G x^2}{k\Delta\check{T}}, \quad L = \frac{R^* D\check{C}_\infty}{k}, \quad M = \frac{\sigma}{\rho U_w}B_0^2 x. \tag{22}$$

Here α_1 and δ are the concentration and temperature difference parameters, and L, Br and N_G are the diffusion parameter, Brinkman number and local entropy generation, respectively.

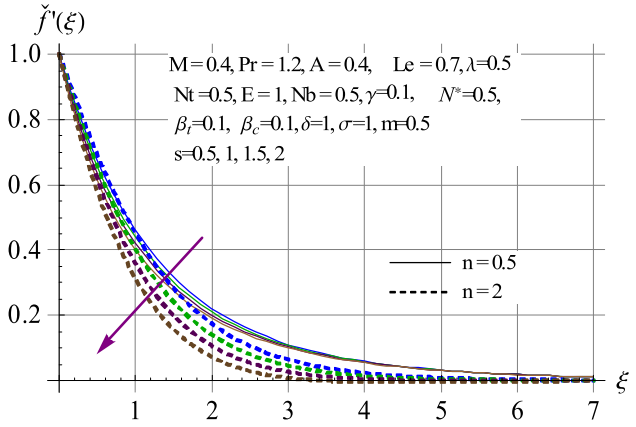

Figure 3. $\breve{f}'(\xi)$ against s.

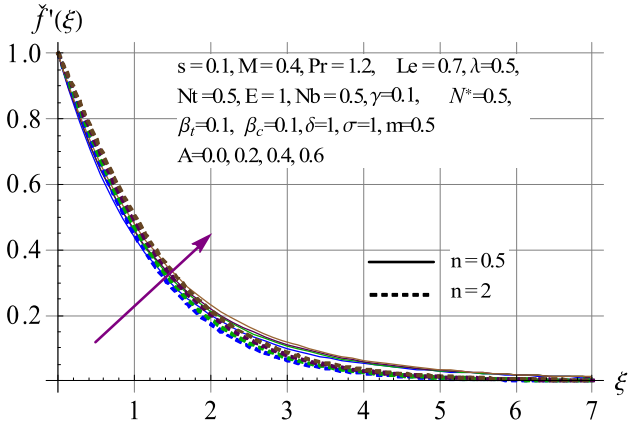

Figure 4. $\breve{f}'(\xi)$ against A.

The dimensionless form of the Bejan number (Be) is

$$\mathrm{Be} = \frac{\text{Entropy generation due to heat and mass transfer}}{\text{Total entropy generation}} \tag{23}$$

In figure 5, as λ and viscous forces are inversely proportional to each other, decline in viscosity is observed for larger λ. This enhances $\breve{f}'(\xi)$. Effects of magnetic field (M) on velocity are shown in figure 6. Velocity decreases for larger M. It is due to the association of

$$\mathrm{Be} = \frac{(\mathrm{Re}_b)^{2/(n+1)}[\delta\breve{\theta}'^2 + L\alpha_1\breve{\theta}'\breve{\phi}' + (L/\delta)\alpha_1^2\breve{\phi}'^2]}{(\mathrm{Re}_b)^{2/(n+1)}[\delta\breve{\theta}'^2 + (\mathrm{Br})\breve{f}''^2 + L\alpha_1\breve{\theta}'\breve{\phi}' + (L/\delta)\alpha_1^2\breve{\phi}'^2] + M(\mathrm{Re}_a)(\mathrm{Br})\breve{f}'^2 + (\mathrm{Re}_a)(\mathrm{Br})(-\breve{f}'')^{n+1}}. \tag{24}$$

6. Discussion

Figures 3–22 are sketched to examine the results of velocity, temperature, concentration, skin friction, Nusselt number, entropy generation and Bejan number for shear thinning ($n < 1$) and thickening ($n > 1$) fluids.

6.1 *Velocity profile*

Figures 3–6 are plotted to examine the behaviour of stretching parameter (s), material constant (A), Hartmann number (M) and mixed convection parameter (λ) on velocity profile ($\breve{f}'(\xi)$). Figure 3 depicts the effect of stretching parameter (s) on $\breve{f}'(\xi)$. It is noted that there is a decay in velocity ($\breve{f}'(\xi)$) for larger values of s in both shear thinning ($0 < n < 1$) and shear thickening ($n > 1$) fluids. Boundary layer of shear thinning fluid is greater than that of the shear thickening fluid due to less viscosity. Figure 4 is portrayed to examine the effects of material parameter (A) on $\breve{f}'(\xi)$ by considering shear thinning and thickening fluids. For larger estimation of A, $\breve{f}'(\xi)$ increases but due to less viscosity, effects of shear thinning fluids are more prominent. Viscous forces diminish for larger A and so $\breve{f}'(\xi)$ enhances. M with Lorentz force which created resistance between fluid particles.

6.2 *Dimensionless temperature*

Figures 7–9 are sketched to show the influence of Pr, Nt, Nb and γ on the temperature ($\breve{\theta}(\xi)$) profile. It is observed that temperature and thermal layer thickness are decreased for both $n < 1$ and $n > 1$. It is due to the enhancement in thermal diffusivity for larger Pr (see figure 7). The impact of Nt on $\breve{\theta}(\xi)$ is shown in figure 8. Temperature ($\breve{\theta}(\xi)$) increases due to fluid particle movement from higher to lower temperature. The impact of thermal slip parameter on temperature is shown in figure 9. Reduction in $\breve{\theta}(\xi)$ is noticed for larger γ.

6.3 *Surface concentration*

Figures 10–14 illustrate the behaviour of Nt and Nb on concentration ($\breve{\phi}(\xi)$). The magnitude of concentration increases and decreases for larger Nt and Nb, respectively (see figures 10 and 11). Collision among fluid particles increases for larger Nb which causes a decrease in $\breve{\phi}(\xi)$. Thermal conductivity increases for

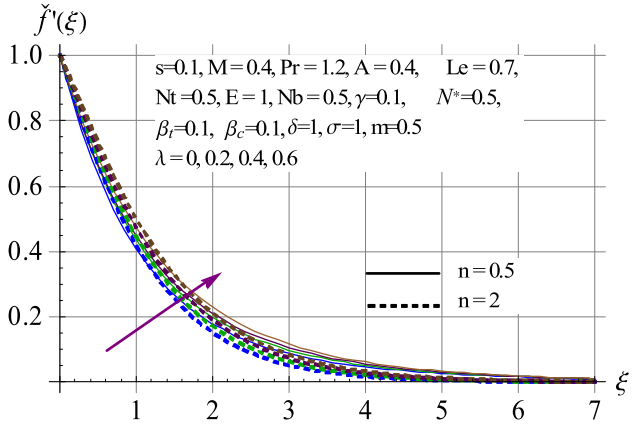

Figure 5. $\breve{f}'(\xi)$ against λ.

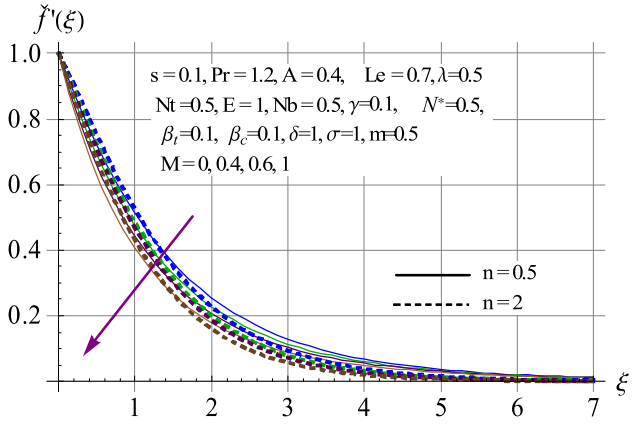

Figure 6. $\breve{f}'(\xi)$ against M.

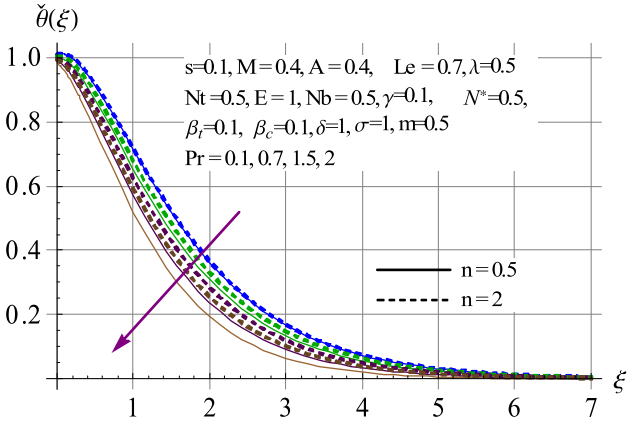

Figure 7. $\breve{\theta}(\xi)$ against Pr.

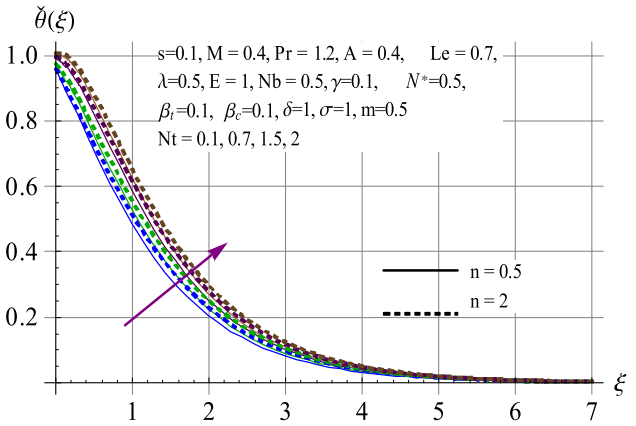

Figure 8. $\breve{\theta}(\xi)$ against Nt.

larger Nt which enhances the boundary layer thickness and concentration. The relationship between activation energy (E) and nanoparticles concentration ($\breve{\phi}(\xi)$) is portrayed in figure 12. The modified Arrhenius function $(\breve{T}/\breve{T}_\infty)^n \exp(-E_a/\kappa\breve{T})$ decreases as activation energy increases which promotes the generative chemical reaction and causes enhancement in $\breve{\phi}(\xi)$. The behaviour of $\breve{\phi}(\xi)$ for varying chemical reaction parameter (σ) is illustrated in figure 13. Concentration ($\breve{\phi}(\xi)$) decreases for larger σ. This behaviour shows weak buoyancy effects due to concentration gradient and consequently, the concentration decreases. Figure 14 shows the behaviour of Le on $\breve{\phi}(\xi)$. A decrease in $\breve{\phi}(\xi)$ is observed for larger Le.

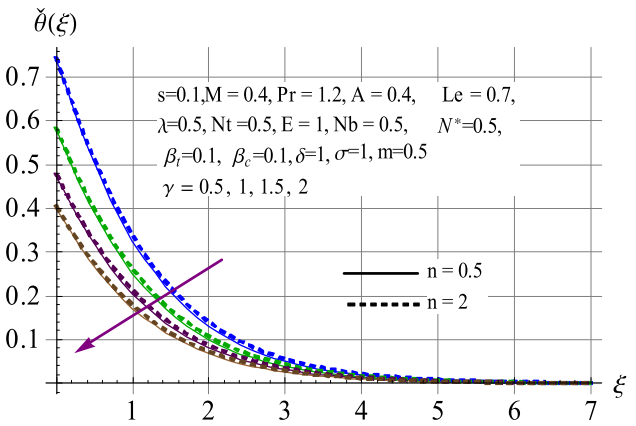

Figure 9. $\breve{\theta}(\xi)$ against γ.

6.4 *Entropy generation and Be*

Figures 15–22 are sketched to examine the behaviour of pertinent variables on N_G and Be. Figures 15 and 16 are plotted to show the behaviour of Br on N_G and Be for comparative study of shear thinning ($n < 1$) and shear thickening ($n > 1$) fluids. The main purpose of Br is to find the heat transfer rate which is released by molecular conduction to viscous heating. It is noted that less heat is released by viscous effect when compared with molecular transfer of heat close to the sheet. However, among the fluid particle layers, a large amount of heat is released which corresponds to an enhancement

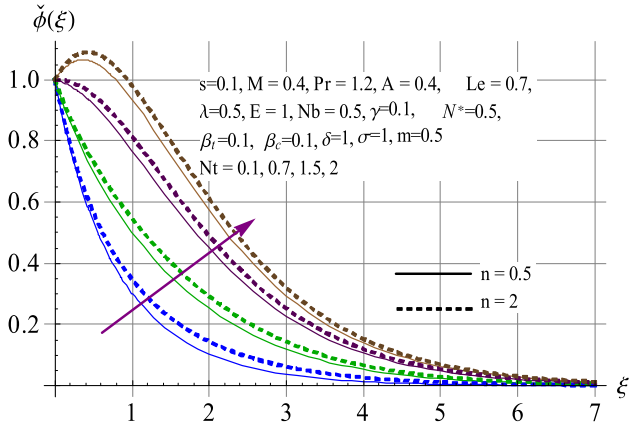

Figure 10. $\breve{\phi}(\xi)$ against *Nt*.

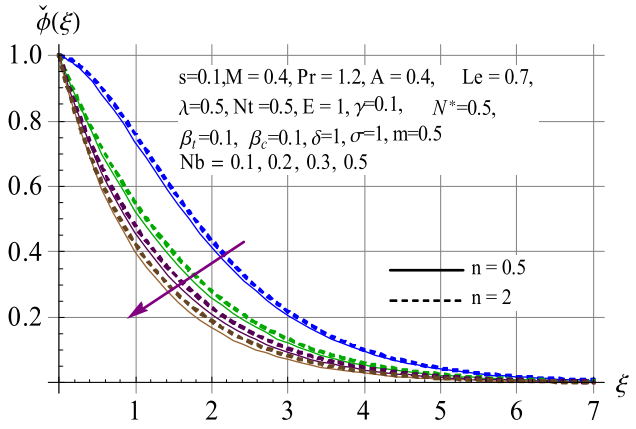

Figure 11. $\breve{\phi}(\xi)$ against *Nb*.

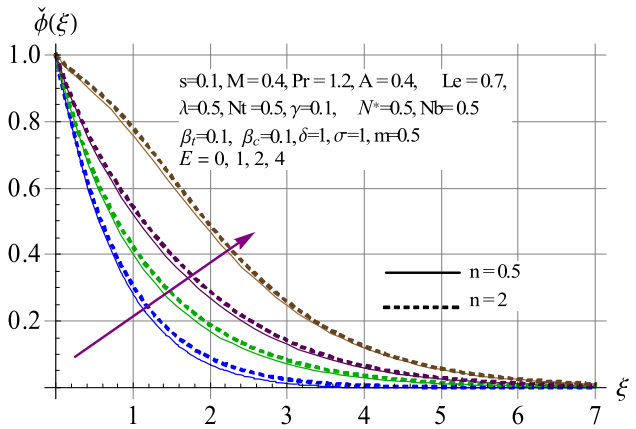

Figure 12. $\breve{\phi}(\xi)$ against *E*.

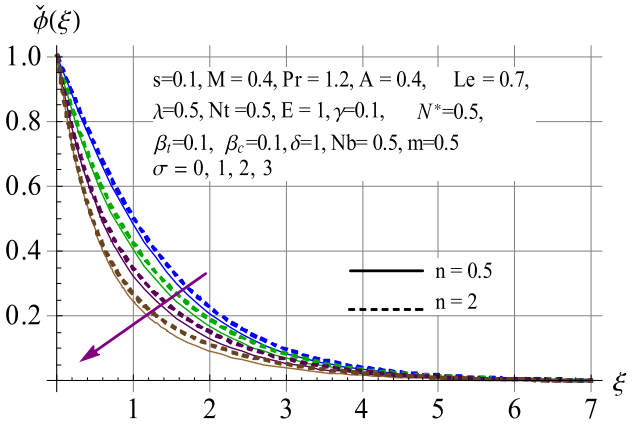

Figure 13. $\breve{\phi}(\xi)$ against σ.

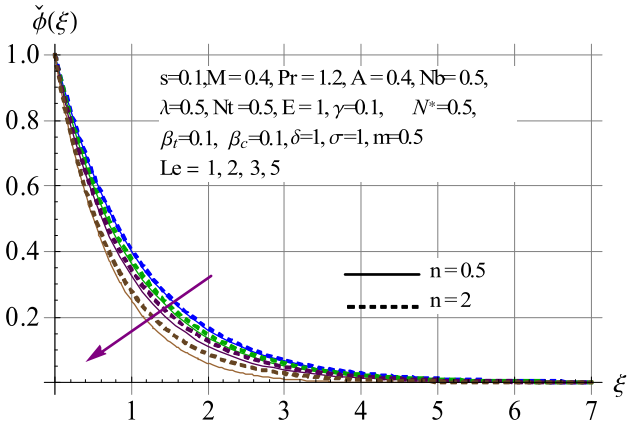

Figure 14. $\breve{\phi}(\xi)$ against Le.

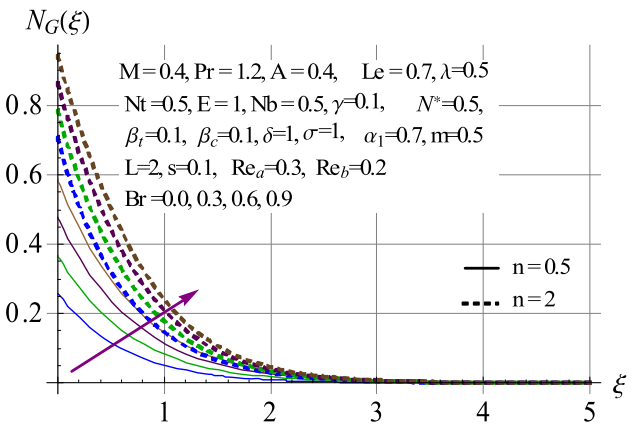

Figure 15. N_G against Br.

in N_G. On the other hand, Be decreases for larger values of Br in both the cases ($n < 1$ and $n > 1$). It shows that viscous effects are more dominant than the effects of heat and mass transfer. Figures 17 and 18 are portrayed to witness the effects of Re_b on N_G and Be in shear thinning and thickening fluids. For larger values of Re_b there is enhancement in N_G while the opposite behaviour of Re_b is noticed for Be. In the case of Be, the effects of shear thickening fluid are more prominent than that of shear thinning fluids. Figures 19 and 20 are sketched to analyse the effect of M on N_G and Be. An opposite behaviour is noticed for both N_G and Be. For larger M, resistance of the fluid enhances due to the enhancement in Lorentz force and consequently,

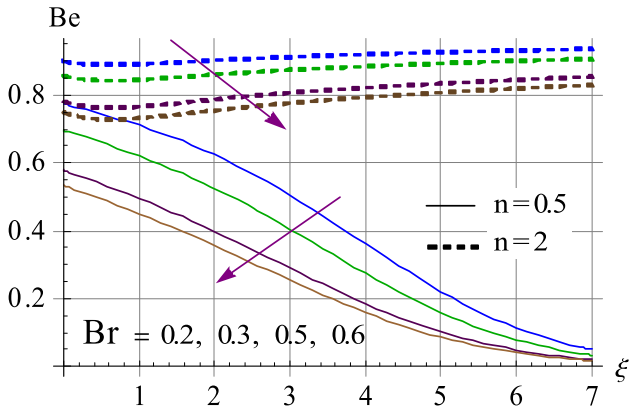

Figure 16. Be against Br.

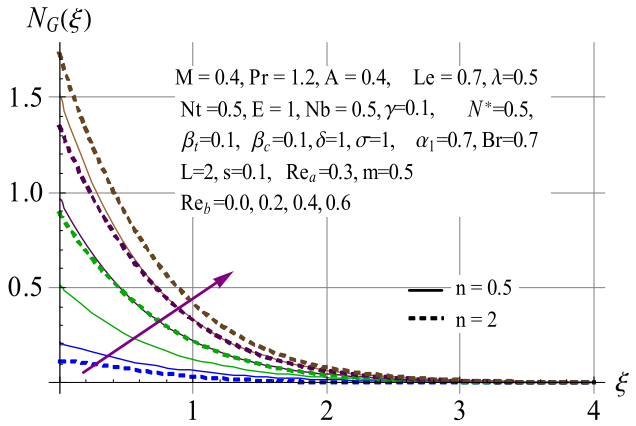

Figure 17. N_G against Re_b.

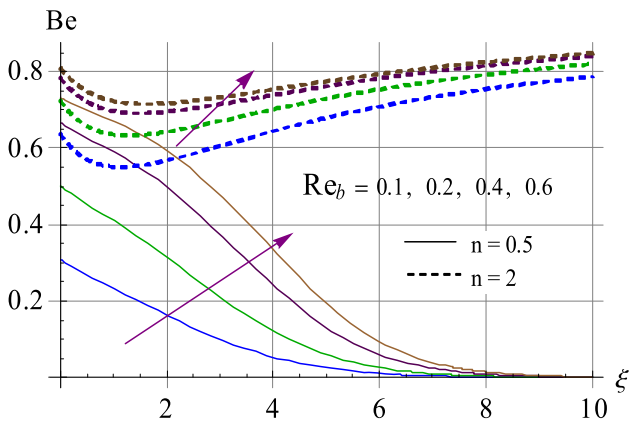

Figure 18. Be against Re_b.

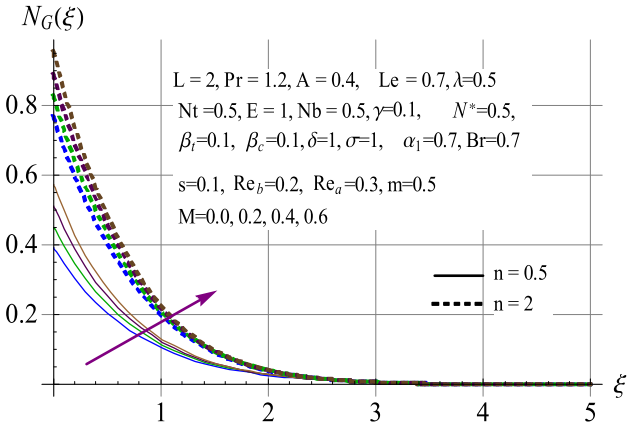

Figure 19. N_G against M.

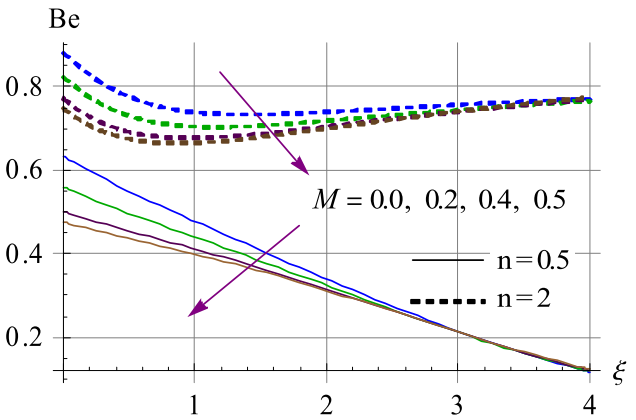

Figure 20. Be against M.

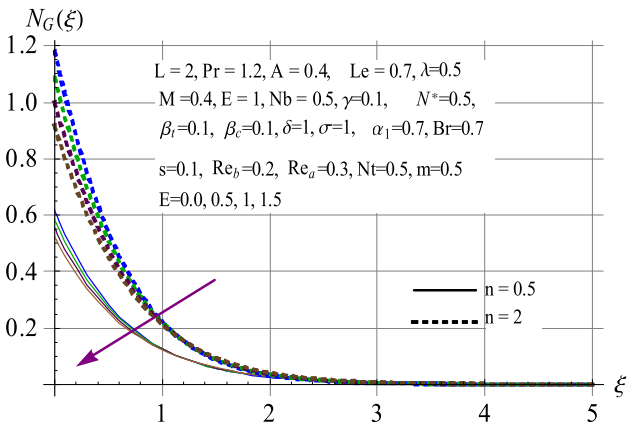

Figure 21. N_G against E.

N_G increases. Be decreases for larger values of M in both the cases ($0 < n < 1$ and $n > 1$) but effects of shear thickening ($n > 1$) fluids are more prominent than the effects of shear thinning ($n < 1$) fluids. This behaviour shows that the irreversibility of fluid friction dominates over the irreversibility of heat and mass transfer. N_G decreases for larger E (see figure 21) in both the cases ($0 < n < 1$ and $n > 1$). But for $n > 1$, there is more viscous dissipation which produces more resistance and as a result more heat loss occurs. That is why effects of shear thickening fluid are more prominent than the effects of shear thinning fluids. On the other hand, for larger E, Be enhances (see figure 22). Be has dual effects, i.e. it decreases near the surface of the sheet

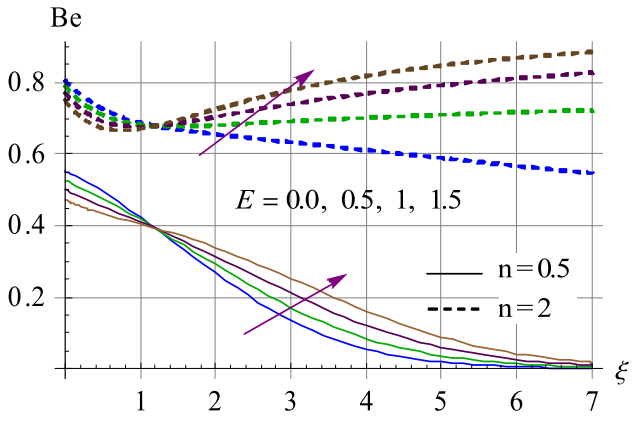

Figure 22. Be against E.

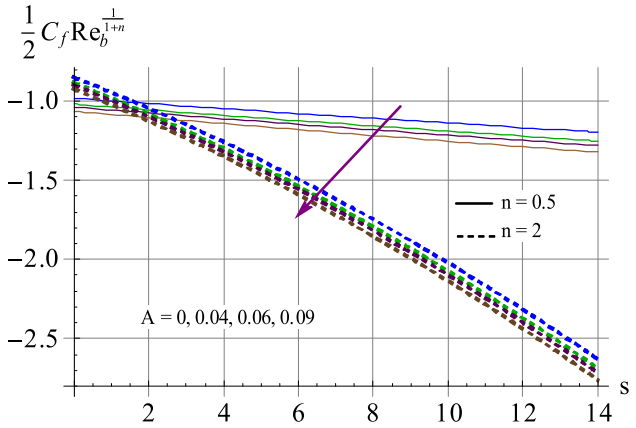

Figure 23. $(1/2)C_f \mathrm{Re}_b^{1/(1+n)}$ against A.

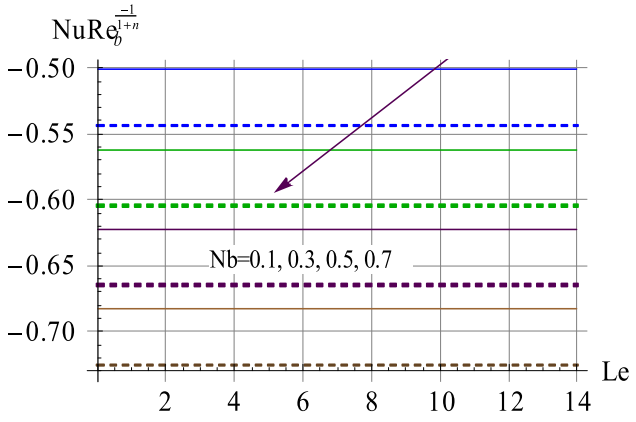

Figure 24. $\mathrm{Re}_b^{-1/(n+1)}\mathrm{Nu}$ against Nb.

while far away from the sheet it increases for both shear thinning and shear thickening of fluids.

6.5 *Skin friction and Nusselt number*

The effects of material parameter (A), Pr, Nt and Nb on skin friction coefficient and Nusselt number are displayed in figures 23 and 24. Figure 23 shows that for larger A, the skin friction increases in shear thinning ($n < 1$) and shear thickening ($n > 1$) fluids. Figure 24 shows that for larger Nb and Nt, the magnitude of rate of heat transfer enhances.

7. Key points

Main observations of the present flow are:

- For A and stretching parameter (s), the opposite behaviour of velocity $\check{f}'(\xi)$ is noticed.
- Temperature profile increases for Nt while it decreases for Pr and γ for both shear thinning and thickening fluids.
- The magnitude of concentration field enhances for higher E and Nt while it reduces via larger Nb.
- There is more N_G for higher values of M, Br and Re_b.
- Be reduces for M and Br while reverse is noticed for Re_b and E.
- For larger A, skin friction increases in shear thinning ($n < 1$) and shear thickening ($n > 1$) fluids.
- Increasing trend for Nusselt number is noticed via Nb.
- N_G and Be are more for shear thickening fluids.

References

[1] A W Sisko, *Ind. Eng. Chem. Res.* **50**, 1789 (1958)
[2] A W Sisko, *J. Colloid Sci.* **15**, 89 (1960)
[3] T Hayat, S Qayyum, M Imtiaz and A Alsaedi, *PLoS ONE* **11(2)**, e0148662 (2016)
[4] R Malik and M Khan, *Result Phys.* **8**, 64 (2018)
[5] M M Bhatti, A Zeeshan and R Ellahi, *Comput. Biol. Med.* **78**, 29 (2016)
[6] M I Khan, T Hayat, M I Khan and A Alsaedi, *Int. Commun. Heat Mass Transf.* **91**, 216 (2018)
[7] M Turkyilmazoglu, *Int. J. Heat Mass Transf.* **8**, 150 (2014)
[8] M Khan, S Munawar and S Abbasbandy, *Int. J. Heat Mass Transf.* **53**, 1290 (2010)
[9] A Tanveer, T Hayat, A Alsaedi and B Ahmad, *J. Mol. Liq.* **236**, 290 (2017)
[10] M I Khan, M Waqas, T Hayat and A Alsaedi, *J. Colloid Interface Sci.* **498**, 85 (2017)
[11] K Ayub, M Y Khan, Q M Hassan, M Ashraf and M Shakeel, *Pramana – J. Phys.* **91**: 83 (2018)
[12] S Choi, *ASME Publ.-Fed* **231**, 99 (1995)
[13] M Mustafa, T Hayat, I Pop, S Asghar and S Obaidat, *Int. J. Heat Mass Transf.* **54**, 5588 (2011)
[14] L Zheng, C Zhang, X Zhang and J Zhang, *J. Frank. Inst.* **350**, 990 (2013)
[15] M Mustafa, J A Khan, T Hayat and A Alsaedi, *J. Mol. Liq.* **211**, 119 (2015)

[16] Y Lin, L Zheng and X Zhang, *Int. J. Heat Mass Transf.* **77**, 708 (2014)
[17] B Mahanthesh, B J Gireesha, R S R Gorla, F M Abbasi and S A Shehzad, *J. Magn. Magn. Mater.* **417**, 189 (2016)
[18] C Yin, L Zheng, C Zhang and X Zhang, *Propuls. Power Res.* **6**, 25 (2017)
[19] D Kumar, J Singh and D Baleanu, *Rom. Rep. Phys.* **69**, 103 (2017)
[20] A K Pandey and M Kumar, *Alex. Eng. J.* **56**, 671 (2017)
[21] A Kumar, R Singh, G Seth and R Tripathi, *Int. J. Heat Technol.* **36**, 1430 (2018)
[22] A Kumar, R Singh, G Seth and R Tripathi, *J. Nanofluids* **7**, 1 (2018)
[23] A R Bestman, *Int. J. Eng. Res.* **14**, 389 (1990), http://dx.doi.org/10.1002/er.4440140403
[24] O D Makinde, P O Olanrewaju and W M Charles, *Afr. Mat.* **22**, 65 (2011)
[25] K A Malique, *J. Thermodyn.* **2013**, 692516 (2013)
[26] Z Abbas, M Sheikh and S S Motsa, *Energy* **95**, 12 (2016)
[27] Z Shafique, M Mustafa and A Mushtaq, *Result Phys.* **6**, 627 (2016)
[28] F G Awad, S Motsa and M Khumalo, *PLoS ONE* **9(9)**, e107622 (2014)
[29] A Bejan, *J. Appl. Phys.* **79**, 1191 (1996)
[30] T Hayat, S Qayyum, M I Khan and A Alsaedi, *Phys. Fluid* **30**, 017101 (2018)
[31] R Ellahi, M Hassan and A Zeeshan, *Int. J. Heat Mass Transf.* **81**, 449 (2015)
[32] A S Butt and A Ali, *J. Brazil. Soc. Mech. Sci. Eng.* **37(1)**, 211 (2015)
[33] J Guo, M Xu, J Cai and X Huai, *Energy* **36**, 5416 (2011)
[34] A Noghrehabadi, M R Saffarian, R Pourrajab and M Ghalambaz, *J. Mech. Sci. Technol.* **27**, 927 (2013)
[35] A Zaib, S Abdelman, A J Chamkha and M M Rashidi, *Heat Transf. Res.* **49(12)**, 1131 (2018), https://doi.org/10.1615/HeatTransRes.201819743
[36] K Ghasemi and M Siavashi, *J. Magn. Magn. Mater.* **442**, 474 (2017)
[37] O D Makinde and A S Eegunjobi, *J. Porous Media* **19**, 799 (2016)
[38] M I Khan, A Kumar and T Hayat, *J. Mol. Liq.* **278**, 677 (2019)
[39] S J Liao, *Homotopy analysis method in nonlinear differential equations* (Springer, Heidelberg, 2012)
[40] M I Khan, S Qayyum, T Hayat and A Alsaedi, *Chin. J. Phys.* **56**, 1525 (2018)
[41] T Hayat, M I Khan, M Farooq, T Yasmeen and A Alsaedi, *J. Mol. Liq.* **220**, 49 (2016)
[42] M Sheikholeslami, M Hatami and D D Ganji, *J. Mol. Liq.* **194**, 30 (2014)
[43] T Hayat, M I Khan, M Farooq, A Alsaedi, M Waqas and T Yasmeen, *Int. J. Heat Mass Transf.* **99**, 702 (2016)
[44] S Qayyum, M I Khan, T Hayat and A Alsaedi, *Physica B* **534**, 173 (2018)
[45] J Sui, L Zheng, X Zhang and G Chen, *Int. J. Heat Mass Transf.* **85**, 1023 (2015)
[46] T Hayat, M I Khan, S Qayyum and A Alsaedi, *Colloids Surf. A: Phys. Eng. Asp.* **539**, 335 (2018)
[47] T Hayat, M I Khan, S Qayyum and A Alsaedi, *Chin. J. Phys.* **55**, 2501 (2017)
[48] A Kumar, R Tripathi, R Singh and G S Seth, *Indian J. Phys.* (2019), https://doi.org/10.1007/s12648-019-01460-4, pp. 1–14
[49] T Hayat, S Qayyum, M I Khan and A Alsaedi, *Int. J. Hydrogen Energy* **42**, 29107 (2017)
[50] T Hayat, M Waqas, S A Shehzad and A Alsaedi, *Pramana – J. Phys.* **86**, 3 (2016)